Josephson vortex lattices as scatterers of terahertz radiation: Giant magneto-optical effect and Doppler effect using terahertz tunable photonic crystals

Sergey Savel'ev,[1,2] A. L. Rakhmanov,[1,3] and Franco Nori[1,4]
[1]*Frontier Research System, The Institute of Physical and Chemical Research (RIKEN), Wako-shi, Saitama, 351-0198, Japan*
[2]*Department of Physics, Loughborough University, Loughborough LE11 3TU, United Kingdom*
[3]*Institute for Theoretical and Applied Electrodynamics, Russian Academy of Sciences, 125412 Moscow, Russia*
[4]*Center for Theoretical Physics, Department of Physics, CSCS, University of Michigan, Ann Arbor, Michigan 48109-1040, USA*
(Received 26 July 2006; published 9 November 2006)

The Josephson vortex (JV) lattice generated by the in-plane magnetic field H_{ab} is a periodic array that scatters Josephson plasma waves (JPWs) in layered superconductors. This produces a photonic band gap structure, i.e. terahertz (THz) photonic crystal, with easily *tunable* forbidden zones, or gaps, controlled either by the in-plane magnetic field or the transverse transport current $J_\perp$ flowing across the superconducting layers. A giant magneto-optical effect, that is a strong dependence of the reflection and transmission coefficients on the applied in-plane magnetic field H_{ab}, is predicted. A relatively small change of H_{ab} can switch the sample from fully transparent to fully reflective within given frequency windows. Thus, the material can change from a THz glass to a mirror by merely changing either H_{ab} or $J_\perp$. The described effects might be useful for development switchable "glass/mirrors" THz filters *tuned* by either H_{ab} or $J_\perp$.

DOI: 10.1103/PhysRevB.74.184512 PACS number(s): 74.25.Qt, 42.70.Qs

I. INTRODUCTION

Layered superconducting structures, including strongly anisotropic (Bi-, Tl-, and Hg-based) high-T_c superconductors (HTS) as well as artificial multilayered heterostructures (e.g., Nb-Al-AlO_x-Nb), exhibit very intriguing physical properties. These layered media can be described as stacks of Josephson junctions (SJJ) and consist of superconducting and insulating layers which are parallel to the crystallographic *ab* plane. The Josephson vortices (JVs) penetrate the sample and form a triangular lattice when the external magnetic field H_{ab} is applied parallel to the *ab* plane. In contrast to Abrikosov or pancake vortices, the interaction between JV and crystal defects is weak and the JV lattice forms a *near-perfect array* of isosceles triangles at low enough temperatures.

It was found[1–4] that the Josephson plasma frequency, ω_J, of HTS layered systems is in the THz range, which is still very difficult to reach for both optic and electronic devices. This is of particular interest for applications[5] and is motivating an increase in studies of high-frequency properties of layered systems. The main focus so far has been on radiation produced by moving either a single JV,[1,6–9] or the entire JV lattice,[3,4] as well as studies of Josephson plasma waves in parallel magnetic fields H_{ab} (Refs. 10–12). For instance, it was predicted that a single Josephson vortex moving through an in-plane-modulated SJJ could emit radiation *within certain frequency windows*,[13] which might be potentially useful for future frequency-selective THz emitters.

The scattering and filtering (i.e., *frequency-selection*) of THz and sub-THz electromagnetic waves (EMWs) using a lattice of vortices inside a layered superconductor were studied in Ref. 14. The vortices were assumed to have very small oscillations under the action of the EMWs. By studying the influence of an almost-fixed JV lattice on the propagation of THz EMWs, it was found that the interaction of the propagating wave and the JV lattice results in forbidden gaps in the frequency spectrum (i.e., THz photonic crystals) conveniently *tunable* by the applied magnetic field H_{ab}. Moreover, by changing H_{ab} one can easily change, by an order of magnitude, the transmission, T, and reflection, $R=1-T$, coefficients of the EMWs. Thus, layered superconducting samples could operate as a THz-frequency filter easily tuned by the applied magnetic field H_{ab}. Recently, in Ref. 15, band-gap structures for a single long Josephson junction were also studied. Note that the reflection and transmission coefficients were not considered in Ref. 15.

This work considers Josephson plasma waves (JPWs) scattering on either *fixed* or *moving* JVs. In Sec. II we analyze a significantly improved model describing the interaction of EMWs and the JV lattice in SJJ. In Sec. III we investigate the band-gap structure (*photonic crystal*) and its evolution when changing the applied magnetic field H_{ab} and the EMW wave vector. In Sec. IV we analyze the propagation of EMWs in the SJJ with a JV lattice. We calculate the dependence of the reflection, $R(H_{ab},\omega)$, and transmission, $T(H_{ab},\omega)$, coefficients on the magnetic field H_{ab} and EMW frequency ω for waves incident on the sample edge from the vacuum. We stress that the in-plane magnetic field H_{ab} drastically affects R and T, even in the absence of band-gap structure. Thus, we predict a giant magneto-optical[16] effect: changing an applied in-plane magnetic field switches the sample from fully transparent (THz *glass*) to fully reflective (THz *mirrors*). In Sec. V we study the effect of the JV lattice motion on the band-gap structure and EMW reflection. We prove that the frequency spectrum of the photonic crystal exhibits a Doppler effect and depends significantly on the velocity of the JVs. Thus, in Sec. V we describe how to use the current $J_\perp$, flowing perpendicular to the layers and driving the JV lattice, to control THz radiation. In Sec. VI we discuss the possibility of experimentally observing the effects described here. A general comparison between usual optical photonic crystals and JV photonic crystals is presented in Table I.

This work significantly extends results briefly summarized in Ref. 14. Namely, here we present a complete deri-

TABLE I. Comparison between standard photonic crystals and tunable THz photonic crystals using Josephson vortices.

	Standard photonic crystals	Josephson-vortex (JV) photonic crystals
Materials	Various (e.g., semiconductors, polymers, insulators)	Layered superconductors (SCs)
Frequency range	Typically optical; Not in THz	Sub-THz and THz
Scatterers	Typically holes in materials	Josephson vortices in SCs
Scatterers made by	An often very complicated and cumbersome fabrication process	Applying H_{ab}
Near-perfect periodicity	Difficult to realize	Automatically provided
Easily tunable?	*No*	*Tunable* via applied magnetic field or current
Moveable scatterers?	No	Yes, producing a Doppler effect
Gap size	Can be large	Typically small
Operating temperature	Typically room temperature	$T<90$ K
Intrinsic nonlinearity	Usually not	Yes, due to nonlinear current-phase relation
Higher harmonic generation	Usually not	Yes, due to nonlinearity
Wave localization	Requires introducing defects	Can be produced by nonlinearities
Magneto-optical effect?	No	Yes

vation of the model describing JV lattices as scatterers of JPWs. This more detailed study uncovers a stronger (by about a factor of 2) magneto-optical effect than was reported earlier.[14] Moreover, here we present a theory describing the scattering of JPW's on driven/moving JV lattices and predict a Doppler-like effect for the band-gap structure and reflection and transmission coefficients.

II. BASIC MODEL

A. Electromagnetic waves in modulated Josephson media

We consider SJJ with layers in the xz coordinate plane [Fig. 1(a)], which coincides with the crystallographic ab plane of the sample in the case of HTS, and the y axis across the layers (along the c axis for HTS). The in-plane magnetic field H_{ab} is applied along the z axis and, thus, the JVs are parallel to the z direction. The JVs form a triangular lattice with distance d_x between vortices within a layer (i.e., along the x direction) and d_y in the y direction. Due to the high anisotropy of the superconducting medium, the distance d_x is much larger than d_y, and $d_x/d_y=\gamma$. Here γ is the anisotropy coefficient of the sample. The usual value of γ for Bi2212 single crystals is about 300–600. As a result, the JV lattice consists of dense vortex rows along the y axis, separated by strips, as schematically shown in Fig. 1(b). We emphasize that the JV lattice at low temperatures is close to an *ideal* isosceles-triangular array, because interactions of JVs with

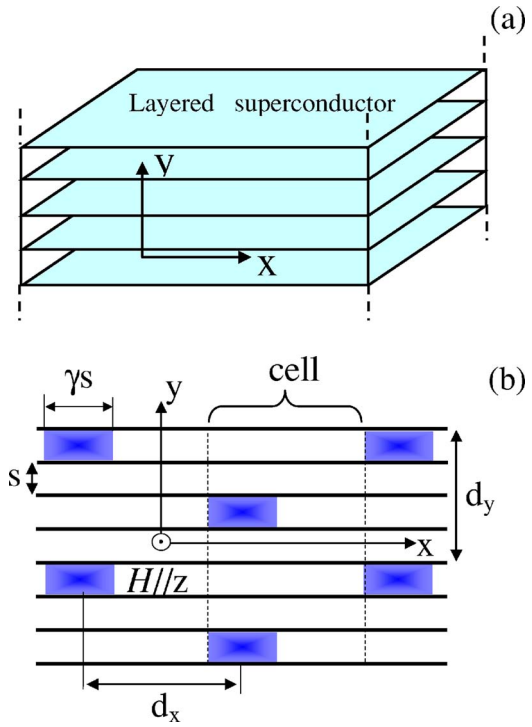

FIG. 1. (Color online) (a) 3D geometry of a layered superconductor with the chosen coordinate system, (b) 2D schematics of the JV lattice with the notation described in the text.

defects are weak due to the absence of the normal-metal core. Note also that the JV lattice can be easily pinned by pancake vortices generated by a weak out-of-plane magnetic field (see, e.g., Ref. 17), which allows an alternative way for tuning JV arrays.

We consider JPW's propagating along the superconducting layers with the magnetic field along the direction of the JV's,

$$\mathbf{H}(x,y,t) = \hat{\mathbf{z}} H_0(x) \exp(iqy - i\omega t), \tag{1}$$

where $\hat{\mathbf{z}}$ is the unit vector along the z axis, q the wave vector perpendicular to superconducting layers, and ω the frequency of the EMWs.

The total tunneling current between the $(n+1)$th and nth superconducting layers is the sum of the pair current and the quasiparticle current caused by the electric field $E_z^{(n)}$. Its density obeys the usual Josephson relation[18]

$$J^{(n)} = J_c \sin(\varphi^{(n)}) + \sigma_\perp E_y^{(n)}, \tag{2}$$

where $\varphi^{(n)}$ is the gauge-invariant interlayer phase difference of the superconducting order parameter in the SJJ, $\sigma_\perp$ is the quasiparticle conductivity in the c-direction, i.e., the direction orthogonal to the CuO_2 layers. The set of coupled sine-Gordon equations for $\varphi^{(n)}$ that corresponds to Eq. (2) can be expressed as[19]

$$\left(1 - \frac{\lambda_{ab}^2}{s^2}\partial_n^2\right)\left(\frac{\partial^2\varphi^{(n)}}{\partial t^2} + \omega_r \frac{\partial\varphi^{(n)}}{\partial t} + \omega_J^2 \sin\varphi^{(n)}\right) - \frac{c^2}{\varepsilon}\frac{\partial^2\varphi^{(n)}}{\partial x^2} = 0. \tag{3}$$

Here λ_{ab} is the London penetration depth across the layers, and s is the interlayer distance (10–20 Å for HTS), the operator ∂_n^2 is defined as $\partial_n^2 f_n = f_{n+1} + f_{n-1} - 2f_n$,

$$\omega_J = \sqrt{\frac{8\pi e s J_c}{\hbar\varepsilon}} \tag{4}$$

is the Josephson plasma frequency, and J_c is the critical current density across the SJJ. The damping frequency, ω_r, can be estimated as $\omega_r = 4\pi\sigma_\perp/\varepsilon$, where ε is the dielectric constant. The transverse conductivity $\sigma_\perp$ is partly controlled by the sample temperature, and the damping can be easily decreased to negligibly small values, $\omega_r/\omega_J \ll 1$. In general, the conductivity along the superconducting layers, $\sigma_\parallel$, should be also included in ω_r.[20,21] However, for frequencies of the order of ω_J, this contribution can be estimated as[22] $\sigma_\parallel/\gamma^2\sigma_\perp \approx 10^{-3}$, and safely omitted. When deriving Eq. (3), the charge neutrality of the system is assumed, which is valid if we are not interested in a frequency range very close to ω_J and wave vectors $|q|$ close to π/s.[19,23,24] Note also that the ω_r-relaxation term in Eq. (3) is small and can be usually neglected. The influence of the dissipation term on the reflectivity and transmissivity is described in Sec. IV B.

We consider the amplitude of the wave $H_0(x)$ to be small compared to the externally applied in-plane field H_{ab} (responsible for generating the JV lattice) and the solution to Eq. (3) can be obtained perturbatively as

$$\varphi^{(n)}(x,t) = \varphi_0^{(n)}(x,t) + \varphi_1(x,y,t), \tag{5}$$

where $\varphi_0^{(n)}(x,t)$ corresponds to the steady JV lattice and small term $\varphi_1(x,y,t)$ describes the propagating EMW. Namely, $|\varphi_1(x,y,t)| \ll |\varphi_0^{(n)}(x,t)|$. Hereafter we assume that φ_1 changes slowly on scales about the distance s between layers, i.e., the discrete phase difference $\varphi_1^{(n)}(x,t) = \varphi_1(x, y=ns, t)$ can be replaced by a continuous function $\varphi_1(x,y,t)$ of y.

The relations between the electric and magnetic fields amplitudes in the EMWs, Eq. (1), and the perturbation of the gauge-invariant phase difference, Eq. (5), are determined by the Maxwell equations and the Josephson relation (2). Using these equations and the charge neutrality condition we can find the following two equations:[19]

$$\frac{\partial E_{0y}^{(n)}}{\partial x} - iqE_{0x}^{(n)} = -\frac{i\omega}{c}H_0^{(n)}, \tag{6}$$

$$E_{0y}^{(n)} = \frac{\Phi_0}{2\pi c s}\frac{\partial\varphi_1}{\partial t}, \tag{7}$$

where $E_{0x}^{(n)}$ and $E_{0y}^{(n)}$ are the corresponding components of the electric field amplitude for the JPWs, and Φ_0 is the flux quantum.

The isolated JV is described by a soliton-like solution of Eq. (3). In layered superconductors, the corresponding equation for the soliton is essentially nonlocal.[8,25] The form of the soliton could not be found explicitly (e.g., Ref. 25). In the junction, where the center of a JV is located, the phase can be approximated as[25]

$$\varphi_0 = \pi + 2\tan^{-1}(x/l_0), \tag{8}$$

where $l_0 = \gamma s$. The phase difference of a soliton decays fast away from the junction having a JV. For moderate magnetic fields, the steady-state solution φ_0 of Eq. (3) can be approximated as a sum,

$$\varphi_0^{(n)}(x) = \sum_m \varphi_0(x - x_{mn}), \tag{9}$$

of isolated solitons. Here x_{mn} is the position of the mth JV in the nth layer. Such an approach is evidently valid if $d_x \gg l_0$. Using the relation $H_{ab} = 2\Phi_0/d_x d_y$ we find the applicability condition of Eq. (9) in the form

$$H_{ab} \ll H_1 = \frac{2\Phi_0}{\gamma s^2}, \tag{10}$$

or $H_{ab} \ll 3$ T, if we take the estimate $\gamma = 600$ and $s = 15$ Å.

Substituting $\varphi_1(x,y,t) = \psi(x)\exp(iqy - i\omega t)$ into Eq. (3), we derive, in the linear approximation:

$$\left[1 + \frac{4\lambda_{ab}^2}{s^2}\sin^2\left(\frac{qs}{2}\right)\right](-\omega^2 - i\omega_r\omega)\psi(x)e^{iqy} + \omega_J^2\psi(x) \times\left(1 - \frac{\lambda_{ab}^2}{s^2}\partial_n^2\right)(e^{iqy}\cos\varphi_0^{(n)}) - \frac{c^2 e^{iqy}}{\varepsilon}\frac{d^2\psi(x)}{dx^2} = 0. \tag{11}$$

B. Limit of long wavelength perpendicular layers

Following Ref. 14, we can reduce the equation set (11) to an ordinary differential equation with respect to $\psi(x)$. Such an approach is valid if the wavelength across the SJJ (along the y direction) is large enough, i.e., the wave vector q is not large. Indeed, from a physical point of view, the JV lattice is equivalent to a *periodic array of scattering centers* across the SJJ (i.e., along the y axis) since $d_y \ll d_x$. The JPW wavelength with $|q|d_y \ll 1$ cannot probe the periodic structure of these scatterers in the y direction, but only their average height and thickness. In other words, the wavelength $2\pi/|q|$ should be larger than the period of the JV's structure in the y direction or in dimensionless form

$$|q|s < 2\pi\sqrt{h_{ab}}, \quad h_{ab} = \frac{H_{ab}}{H_1}. \tag{12}$$

For HTS like Bi2212, the value of the characteristic field $H_1 = 2\Phi_0/\gamma s^2$ is of the order of 3–6 T.

Mathematically, the procedure of averaging Eq. (11) can be performed as in usual electrodynamics of continuous media.[26] In Eq. (11) we should average the term with the operator ∂_n^2 which acts on the product of the fast-varying "microscopic" value $\cos\varphi_0^{(n)}$ and the slowly varying wave e^{iqy} (here, "fast/slowly" refers on the variation along the y axis). Using a straightforward transformation we find $\partial_n^2(f_n g_n) = g_n\partial_n^2 f_n + \partial_n^f f_n \partial_n^f g_n + \partial_n^b f_n \partial_n^b g_n + f_n \partial_n^2 g_n$, where the corresponding forward and backward derivatives are $\partial_n^f f_n = f_n - f_{n-1}$ and $\partial_n^b f_n = f_n - f_{n+1}$. Applying the last rule to $\partial_n^2(e^{iqy}\cos\varphi_0^{(n)})$ we find, under the condition (12), the following result:

$$\partial_n^2(e^{iqy}\cos\varphi_0^{(n)}) = -(qs)^2 e^{iqy}\cos\varphi_0^{(n)} + e^{iqy} \times (F.D.), \tag{13}$$

where the symbol $(F.D.)$ denotes a sum of terms containing "full differentials," ∂_n, of the fast-varying function $\cos\varphi_0^{(n)}$. The average of the first term in the right-hand side of Eq. (13) includes the average value of $\cos\varphi_0^{(n)}$,

$$\langle\cos\varphi_0^{(n)}\rangle = \frac{1}{2N}\sum_{l=n-N}^{n+N}\cos\varphi_0^{(l)}, \tag{14}$$

while the average of the sign-alternating fast-varying functions $(F.D.)$ is zero. Thus,

$$\langle\partial_n^2(e^{iqy}\cos\varphi_0^{(n)})\rangle \approx -(qs)^2 e^{iqy}\langle\cos\varphi_0^{(n)}\rangle, \tag{15}$$

where $\langle\ldots\rangle$ means average along the y direction.

In the long wavelength limit we have $\sin^2(qs/2) = (qs/2)^2$, and the averaged Eq. (11) can be written in the form[14]

$$(1+\lambda_{ab}^2 q^2)(\omega_J^2\langle\cos\varphi_0^{(n)}\rangle - \omega^2 - i\omega\omega_r)\psi - \frac{c^2}{\varepsilon}\frac{d^2\psi}{dx^2} = 0. \tag{16}$$

We introduce the dimensionless variables

$$\eta = \frac{x}{\gamma s}, \quad \tilde{\omega} = \frac{\omega}{\omega_J}, \quad \tilde{\omega}_J(\eta) = \langle\cos\varphi_0^{(n)}\rangle,$$

$$\tilde{\omega}_r = \frac{\omega_r}{\omega_J}, \quad \kappa_0^2(q) = \left(\frac{s}{\lambda_{ab}}\right)^2(1+q^2\lambda_{ab}^2). \tag{17}$$

Now, using the relations $\lambda_c = c/\sqrt{\varepsilon}\omega_J$ and $\lambda_c/\lambda_{ab} = \gamma$, we can rewrite Eq. (16) in a dimensionless form

$$\psi''(\eta) - \kappa_0^2(q)[\tilde{\omega}_J^2(\eta) - \tilde{\omega}^2 - i\tilde{\omega}\tilde{\omega}_r]\psi(\eta) = 0, \tag{18}$$

where the prime denotes the differentiation with respect to η. The function $\tilde{\omega}_J^2(\eta)$ has a field-tunable period

$$d_x/\gamma s = 1/\sqrt{h_{ab}}. \tag{19}$$

The physical meaning of the function $\tilde{\omega}_J(\eta)$ is the modulation of the Josephson frequency, since the effective critical current of the layered medium becomes modulated due to the current suppression near the JV cores.

C. Stepwise approximation for Josephson vortex cores

Equation (18) is an ordinary linear differential equation with periodic coefficients. It can be studied numerically. Alternatively, this equation can be considered as a Schrödinger equation with a periodic "potential" $\tilde{\omega}_J^2(\eta)$. Then, well-known analytical methods can be used to find the "zone" or *gap structure* of the system, as well as the reflection and transition coefficients. In particular, Eq. (18) could be approximately solved by the WKB method. However, we can use the method proposed in Ref. 14, which seems to us to be more appropriate for the qualitative analysis of the scattering of JPWs by JVs. Namely, we approximate $\tilde{\omega}_J^2(\eta)$ by a stepwise function.

To find an appropriate approximation for $\tilde{\omega}_J^2(\eta)$, we now briefly describe the structure of an isolated JV. In the junction where a JV is located, i.e., inside and around a JV, we derive

$$\cos\varphi_0^{(0)}(x) = -\frac{l_0^2 - x^2}{l_0^2 + x^2}, \tag{20}$$

from Eq. (8). The profile of $\cos\varphi_0^{(0)}(x)$ is shown in Fig. 2 by a red continuous line. The approximate stepwise potential well $W(x)$ with the size $2l_0$ for this profile is shown by the dashed blue line. The height of the stepwise function is chosen from the condition $\int_{-\infty}^{\infty} W(x)dx = \int_{-\infty}^{\infty}\cos\varphi_0^{(0)}(x)dx$. Thus, we obtain $W(x) = 1 - \pi F(x)$, where $F(x) = 1$, if $|x| < l_0$, and $F(x) = 0$, otherwise.

It follows from Eq. (3) that the soliton solution decays rapidly away from the contact having a JV. Then, we can neglect φ compared with $(\lambda_{ab}^2/s^2)\partial_n^2\varphi$ in this equation. Thus, we derive

$$\partial_n^2\sin\varphi_0^{(n)} \approx -\gamma^2 s^2\frac{\partial^2\varphi_0^{(n)}}{\partial x^2}. \tag{21}$$

Solving this equation we find

$$\sin\varphi_0^{(\pm 1)} = \sin\varphi_0^{(0)}\left(\frac{x^2}{x^2 + l_0^2}\right) \tag{22}$$

for the phase difference in the junctions next to the "0"th contact. Thus, the value of $\cos\varphi_0$ decreases considerably

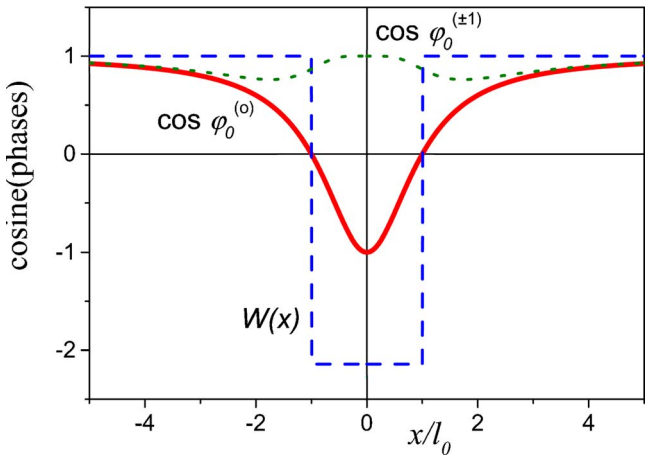

FIG. 2. (Color online) Spatial distributions, near the vortex core, of the cosine of the phase differences: the red continuous line denotes cos $\varphi_0^{(0)}(x)$, the dotted green line corresponds to cos $\varphi_0^{(\pm1)}(x)$, and the blue dashed line shows the approximant $W(x)$. $\varphi_0^{(0)}(x)$ refers to the phase difference in the junction having a JV, while $\varphi_0^{(\pm1)}(x)$ corresponds to the neighboring junctions.

even in the layers nearest to the contact with a soliton, the green dotted line in Fig. 2. Thus, we assume that the effective thickness of the JV is s. As a result, we find the approximate expression for the function $\tilde{\omega}_J^2(\eta)$ in the form[27]

$$\tilde{\omega}_J^2(\eta) = 1 - \pi h_{ab}^{1/2} \sum_m F\left(\eta - \frac{m}{\sqrt{h_{ab}}}\right), \tag{23}$$

where $F(\eta)=1$, if $|\eta|<1$, and $F=0$, if $|\eta|>1$, and we use the relation $2\Phi_0/(d_x d_y)=H_{ab}$.

The second order differential equation (18) requires the continuity of the functions $\psi(\eta)$ and $\psi'(\eta)$ in the sample, for the continuity of the corresponding components of the electromagnetic field.

III. BAND-GAP STRUCTURE

Forbidden zones in the $\omega(k)$ dependence, or so-called "photonic crystal,"[28–32] can occur when EMWs propagate through a periodically modulated structure. For layered superconductors, the JV lattice can serve as such a periodical scattering structure.[14] The period of the JV lattice can be easily tuned by the applied magnetic field H_{ab}, which is convenient for experimental realizations of *JPW photonic crystals* and also of significance for possible applications as *tunable THz filters*.

In this section we neglect, for simplicity, the relaxation term in Eq. (18) since ω_r is much lower than ω_J. The validity of this approximation can be derived directly from Eq. (18). We find from this equation that (in dimensional units) the characteristic decay length of the EMW's is about

$$l_r = \frac{\sqrt{2}\gamma s \omega_J}{\kappa_0(q)\sqrt{\omega\omega_r}}. \tag{24}$$

Taking for estimates the standard parameters for Bi2212, $\gamma=500$, $s=1.5$ nm, $\omega_r/\omega_J=10^{-6}$, we find that $l_r \approx 2.5$ mm even for the largest value of $qs=0.3\pi$ we treated. The obtained length l_r is of the order of the usual sizes for Bi2212 single crystals and much larger than the scale of the JV structure in any reasonable magnetic field. This justifies our approximation.

The spatial period of the JVs structure is d_x in the x direction, or $1/\sqrt{h_{ab}}$ in dimensionless units. Following the usual band-theory approach for electrons in crystal lattices, we seek the solution of Eq. (18) in the form of a Bloch wave $\psi(\eta)=u(\eta,k)\exp(ik\eta)$, where $u(\eta,k)$ is a periodic function of η with the period of the JV lattice and the dimensionless wave vector k is in the first Brillouin zone, $-\pi\sqrt{h_{ab}}<k<\pi\sqrt{h_{ab}}$.

Consider the jth elementary cell, $\eta_j<\eta<\eta_j+1/\sqrt{h_{ab}}$, shown in Fig. 1(b). The solution $\psi(\eta)$ of the linear Eq. (18) (either within the JV core, $\eta_j<\eta<\eta_j+1$, or outside the core, $\eta_j+1<\eta<\eta_j+1/\sqrt{h_{ab}}$), is a sum of exponential terms

$$\psi_j = C_{1j}^l e^{i\kappa_l \eta} + C_{2j}^l e^{-i\kappa_l \eta}, \tag{25}$$

where C_{1j}^l and C_{2j}^l are constants, $l=1$ corresponds to the space between JVs, and $l=2$ corresponds the space inside JV cores,

$$\kappa_1 = \kappa_0\sqrt{\tilde{\omega}^2 - 1}, \quad \kappa_2 = \kappa_0(\tilde{\omega}^2 + \pi\sqrt{h_{ab}} - 1)^{1/2}. \tag{26}$$

Using the continuity of ψ and ψ' at the cores' boundary and the periodicity of the Bloch functions and its derivatives, we obtain a set of homogeneous linear equations for C_{1j}^l and C_{2j}^l

$$C_{1j}^1 + C_{2j}^1 = C_{1j}^2 + C_{2j}^2, \quad \kappa_1 C_{1j}^1 - \kappa_1 C_{2j}^1 = \kappa_2 C_{1j}^2 - \kappa_2 C_{2j}^2,$$

$$e^{ikb}(C_{1j}^1 e^{-i\kappa_1 b} + C_{2j}^1 e^{i\kappa_1 b}) = e^{-ik}(C_{1j}^2 e^{i\kappa_2} + C_{2j}^2 e^{-i\kappa_2}),$$

$$e^{ikb}[(\kappa_1 - k)C_{1j}^1 e^{-i\kappa_1 b} - (\kappa_1 + k)C_{2j}^1 e^{i\kappa_1 b}] = e^{-ik}[(\kappa_2 - k)C_{1j}^2 e^{i\kappa_2} - (\kappa_2 + k)C_{2j}^2 e^{-i\kappa_2}],$$

where $b=1/\sqrt{h_{ab}}-1$ and $-\pi<k(b+1)<-\pi$. The nontrivial solution of these equations exists only if their determinant is zero. Then, after straightforward algebra, we obtain the dispersion equation for the frequency $\tilde{\omega}(k)$ in the form

$$\cos(\kappa_1 b)\cos(\kappa_2) - \frac{\kappa_1^2 + \kappa_2^2}{2\kappa_1\kappa_2}\sin(\kappa_1 b)\sin(\kappa_2) = \cos[k(b+1)]. \tag{27}$$

We can find the spectrum $\tilde{\omega}(k)$ by solving Eq. (27). This spectrum is shown in Fig. 3 for different values of the wave vectors q and applied magnetic fields. In the presence of an applied magnetic field, two particular features of the spectrum $\tilde{\omega}(k)$ should be emphasized. First, the propagation of EMWs in the system is possible at frequencies lower than ω_J, due to the periodic suppression of the critical current in the cores of the JVs. Second, the gap in the spectrum, or forbidden frequency band, is maximum when $\lambda_y \sim s$ and for intermediate fields h_{ab}. The dependence of the band-gap structure for growing q and H_{ab} can be easily understood as follows. The number of JVs increases when increasing the applied in-plane magnetic field, while the effective interaction between the EMWs and the JVs increases for the grow-

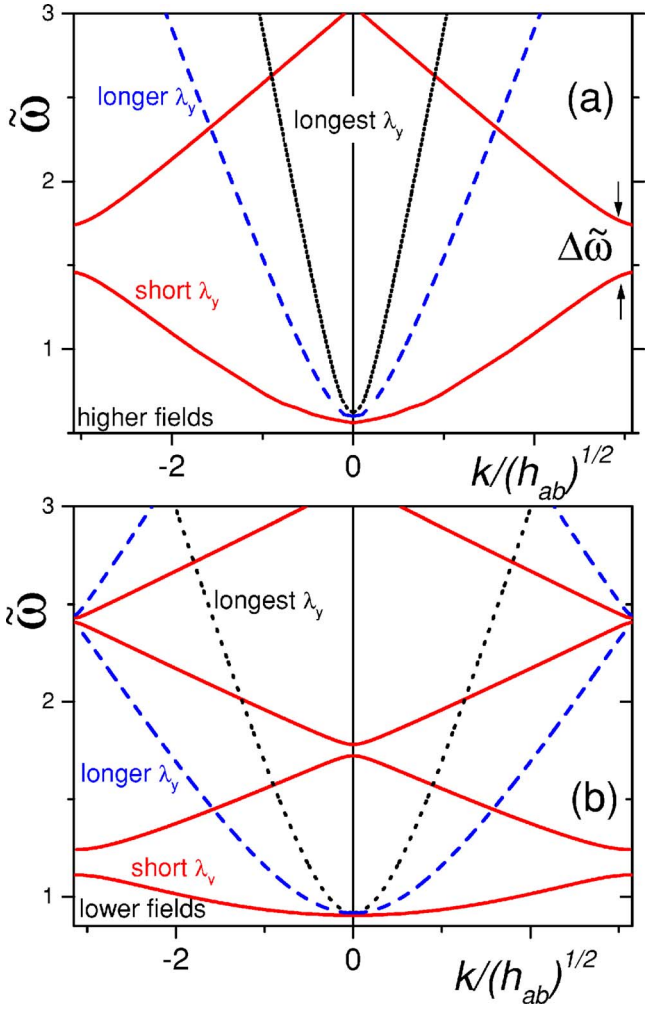

FIG. 3. (Color online) Band-gap structure of an EMW propagating in a layered superconductor with a JV lattice: Frequency $\tilde{\omega}$ of the EMW versus $k(h_{ab})^{-1/2}$ at $h_{ab}=0.2$ (a) and at a lower field $h_{ab}=0.05$ (b) for different wavelengths $\lambda_y=1/q$: $qs=0.3\pi$ (red solid line) and $qs=0.1\pi$ (blue dashed line) and $qs=0.05\pi$ (black dotted curve). The frequency gap (forbidden frequency range) between the first and the second zone is indicated by $\Delta\tilde{\omega}\approx 0.2$. This gap $\Delta\tilde{\omega}$ diminishes for smaller q ($q=y$-axis wave vector). Here, we use $s=15$ Å, $\lambda_{ab}=2000$ Å, $\gamma=600$ and $\tilde{\omega}_r=0$.

ing q and H_{ab}, consistent with Eqs. (27) and (26). According to the well-known criterium for the existence of photonic crystals,[29–32] the band-gap structure in the EMW spectrum occurs if the concentration of periodic inhomogeneities is high enough and the optical properties of these inhomogeneities differ considerably from that of the ambient matter. It could be concluded that there should exist an optimum value of the applied field h_{ab} for the observation of photonic crystals in layered superconductors. At this field, the part of the space occupied by the vortex cores should be about half of the total volume. However, when h_{ab} is of the order of unity our analytical approach is not applicable and further numerical studies would be useful. Note also that $\Delta\omega$ decreases fast when the number of the frequency zone increases, as shown in Fig. 3.

The spectrum shown in Fig. 3 could be directly measured in experiments studying nonlinear effects[22] in plasma wave

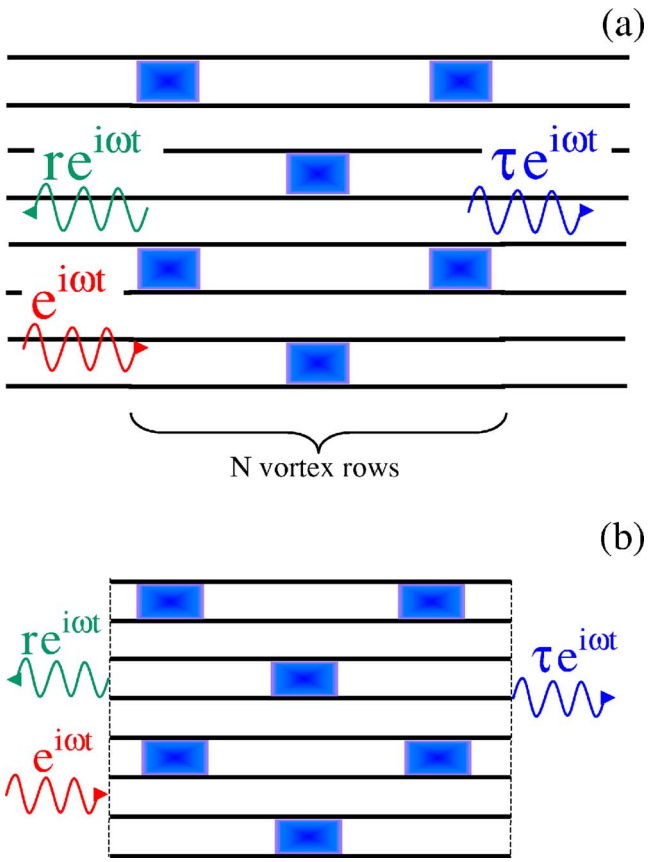

FIG. 4. (Color online) Schematic diagram of the EMW's interacting with a JV lattice. (a) Internal reflection of the EMW emitted, e.g., by a JV. (b) The EMW is incident from outside the sample.

propagation. Indeed, higher-harmonic generation should be sensitive if their frequencies occur within a frequency gap. Other nonlinear effects, including self-induced transparency or light slowing down, can be strongly enhanced due to the photonic crystal spectrum of the JPWs.

IV. PLASMA WAVE REFLECTIVITY TUNED BY THE IN-PLANE MAGNETIC FIELD

The possibility of producing a THz photonic crystal in the SJJ, due to presence of JVs, indicates that the JV lattice can significantly affect the reflectivity and transparency of layered superconductors. Here we calculate the transmission and reflection coefficients for two cases:

(i) EMWs propagating inside the sample as shown in Fig. 4(a); such a wave can be emitted by some internal source, e.g., by a moving JV.

(ii) EMW's incident on the sample from the vacuum and propagating through the SJJ, as shown in Fig. 4(b).

As a result of our calculation (see subsections below), we derive the strong dependence of the reflection and transmission coefficients, shown in Fig. 5 and 6, on the applied in-plane magnetic field H_{ab}. A relatively small change (about 10–100 Oe) in H_{ab} can switch the sample from *fully transparent* (THz glass) to *fully reflected* (THz mirror) regimes

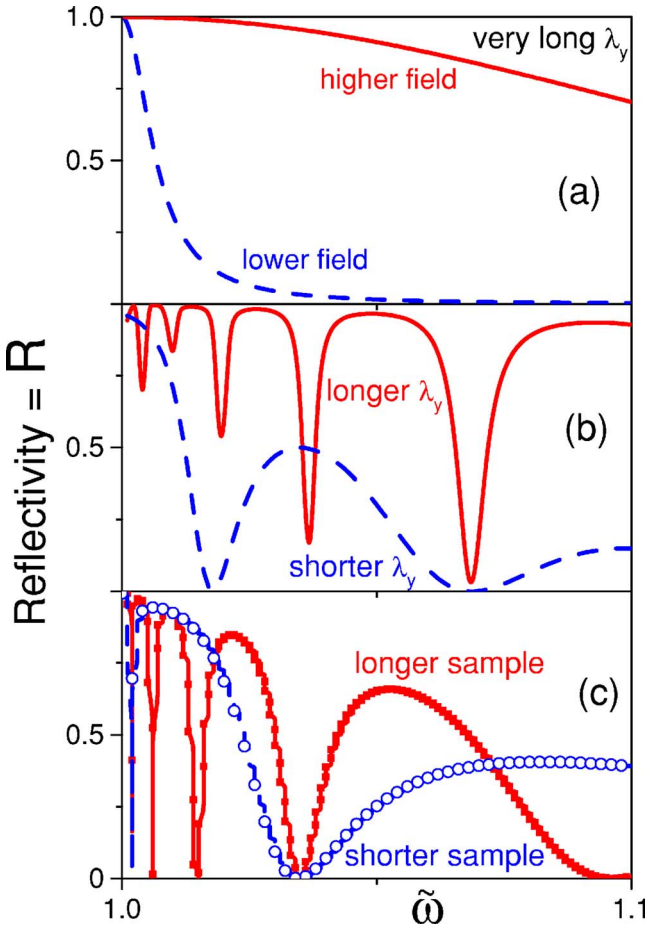

FIG. 5. (Color online) Internal reflection: EMWs emitted (by a moving JV) inside a sample [Fig. 4(a)] reflect back with intensity $R=|r|^2$ and transmit forward with intensity $T=|\tau|^2=1-R$. The reflection coefficient R versus the EMW frequency $\tilde{\omega}$ for (a) a sample with length $l=100\gamma s$ at $qs=0$ for $h_{ab}=10^{-4}$ (blue dashed line) and 25 times larger field $h_{ab}=2.5\times10^{-3}$ (red solid line); notice that here the wavelength $\lambda_y\to\infty$ along the y axis and, thus, the reflectivity monotonically decreases with frequency; (b) $l=100\gamma s$ at $h_{ab}=4\times10^{-2}$ for $qs=0.1\pi$ (red solid line) and shorter $qs=0.3\pi$ (blue dashed line); here notice that the case $qs=0.1\pi$ case has a larger number of minima in $R(\omega)$; (c) $h_{ab}=2.5\times10^{-3}$ and $qs=0.05\pi$ for a sample with length $l=100\gamma s$ (blue open circles) and $l=600\gamma s$ (red solid squares); here the length of the sample is changed. For our calculations, we use $s=15$ Å, $\lambda_{ab}=2000$ Å, $\gamma=600$ and $\tilde{\omega}_r=10^{-6}$.

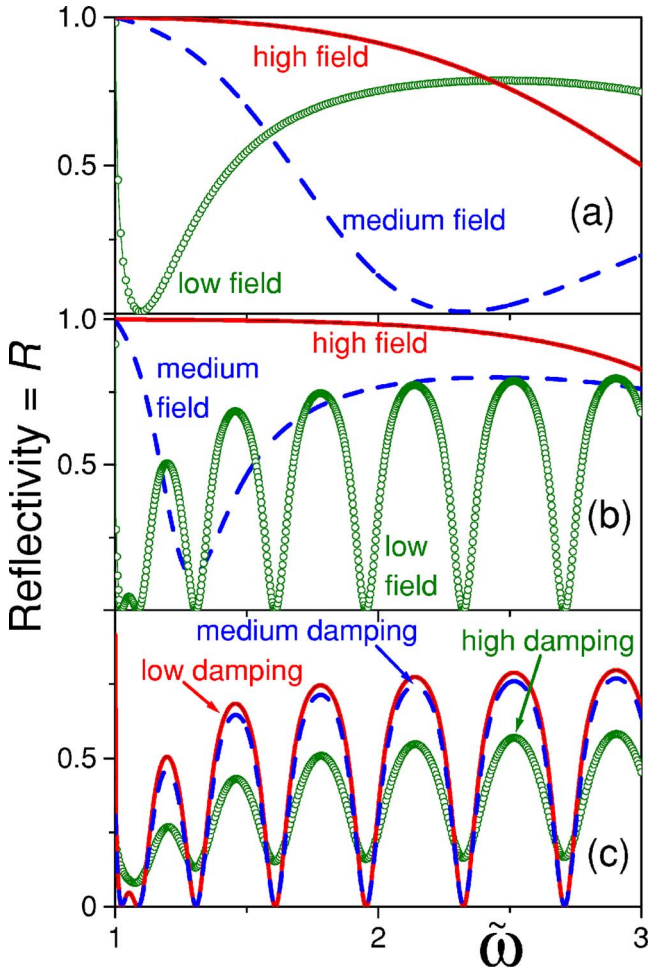

FIG. 6. (Color online) Reflection of electromagnetic waves from the sample, or THz tunable filter shown in Fig. 4(b). The reflection coefficient R versus $\tilde{\omega}$ for an EMW propagating from the vacuum at $q=0$, (a) for $l=100\gamma s$, $\tilde{\omega}_r=10^{-6}$ and different in-plane magnetic fields $h_{ab}=10^{-4}$ (green circles), $h_{ab}=2.5\times10^{-3}$ (blue dashed line), $h_{ab}=10^{-2}$ (top red solid line); (b) for $l=1000\gamma s$, $\tilde{\omega}_r=10^{-6}$, and $h_{ab}=0$ (green circles), $h_{ab}=10^{-4}$ (blue dashed line), $h_{ab}=2.5\cdot10^{-3}$ (top red solid line); and (c) for $l=1000\gamma s$ and $h_{ab}=0$ and varying the damping $\tilde{\omega}_r$ with $\tilde{\omega}_r=10^{-6}$ (top red solid line), $\tilde{\omega}_r=10^{-2}$ (blue dashed line), $\tilde{\omega}_r=10^{-1}$ (green circles). Other parameters are the same as in Fig. 5. The deep minima for the solid line in (b) are due to the reflection at the sample boundaries.

within a given frequency window. Therefore, the optical characteristics of layered superconductors can be conveniently tuned by the in-plane magnetic field. Thus, we predict a giant magneto-optical effect.

A. Electromagnetic waves propagating inside the sample

In this case, EMWs are not scattered by sample boundaries and we calculate the reflectivity (or transparency) for JPWs passing through the JV lattice, which includes N rows of JVs. The length of the considered array of JV scatterers is

$$l=\gamma sN/\sqrt{h_{ab}}. \tag{28}$$

The wave vector q of the EMWs described in Eq. (1) can have any value allowed by the dispersion law in the SJJ. However, we should restrict our consideration to $|qs|\ll\pi$ when using the continuum approximation. The relation between the amplitudes of the EMWs and the gauge-invariant phase difference is linear.[18] Thus, here we can calculate the transparency and reflection coefficients for the wave ψ. In contrast to the previous section, we now seek nonperiodic solutions of Eq. (18).

Solution (25), $\psi_j=\vec{e}\cdot\vec{\psi}_j^{\,l}$ with $\vec{e}=(1,1)$, of Eq. (18) for the jth cell of the magnetic structure can be expressed in a vector form as

$$\vec{\psi}_j^l = \{C_{1j}^l \exp(i\kappa_l \eta);\ C_{2j}^l \exp(-i\kappa_l \eta)\}, \tag{29}$$

where κ_l is determined from Eq. (26). However, in this section we take into account the relaxation term in Eq. (18). So, we replace κ_l in Eq. (26) by

$$\kappa_1 = \kappa_0(\tilde{\omega}^2 - 1 + i\tilde{\omega}\tilde{\omega}_r)^{1/2},$$

$$\kappa_2 = \kappa_0(\tilde{\omega}^2 + \pi\sqrt{h_{ab}} - 1 + i\tilde{\omega}\tilde{\omega}_r)^{1/2}. \tag{30}$$

The continuity of ψ and ψ' results in a set of linear equations relating $\vec{\psi}_\alpha^{j-1}$ and $\vec{\psi}_\alpha^{j}$. This can be written in matrix form as

$$\hat{A}_1 \vec{\psi}_1^{j-1} = \hat{A}_2 \vec{\psi}_2^{j}, \quad \hat{B}_2 \vec{\psi}_2^{j} = \hat{B}_1 \vec{\psi}_1^{j} \tag{31}$$

where

$$\hat{A}_\alpha = \begin{pmatrix} 1 & 1 \\ i\kappa_\alpha & -i\kappa_\alpha \end{pmatrix}, \quad \hat{B}_\alpha = \begin{pmatrix} e^{i\kappa_\alpha b} & e^{-i\kappa_\alpha b} \\ i\kappa_\alpha e^{i\kappa_\alpha b} & -i\kappa_\alpha e^{-i\kappa_\alpha b} \end{pmatrix}.$$

The solution of these equations can be written in a symbolic form $\vec{\psi}_\alpha^{j} = \hat{L}\vec{\psi}_\alpha^{j-1}$, where $\hat{L} = \hat{B}_1^{-1}\hat{B}_2\hat{A}_2^{-1}\hat{A}_1$. Then, we use a linear nondegenerate transformation

$$\hat{G} = \begin{pmatrix} 1 & \beta_1 \\ \beta_2 & 1 \end{pmatrix}$$

that diagonalizes $\hat{L}$. Here

$$\beta_{1,2} = \pm \frac{M_2 - M_1 + \sqrt{(M_2 - M_1)^2 + 4L_1L_2}}{2L_{1,2}},$$

$$M_{1,2} = \left[\cos \kappa_2(b-1) \pm i\frac{\kappa_1^2 + \kappa_2^2}{2\kappa_1\kappa_2} \sin \kappa_2(b-1)\right] e^{\mp i(b-1)\kappa_1},$$

$$L_{1,2} = \pm i\frac{\kappa_1^2 - \kappa_2^2}{2\kappa_1\kappa_2} \sin \kappa_2(b-1) e^{\pm i(b-1)\kappa_1}. \tag{32}$$

By applying N times such a procedure, we find the linear transformation

$$\vec{\psi}_\alpha^{N} = \hat{G}^{-1}(\hat{G}\hat{L}\hat{G}^{-1})^N \hat{G}\vec{\psi}_\alpha^{0} \tag{33}$$

that propagates the solution from the 0th to Nth elementary cell.

Next, we calculate the reflection and transmission coefficients. We denote the amplitude of the incident wave C_{10}^1 as 1, the amplitude of the reflected wave C_{10}^2 as r, and the amplitude of the transmitted wave C_{1N}^1 as τ [Fig. 4(a)]. Using Eq. (33) we obtain two linear equations for two independent variables, r and τ, since $C_{1N}^2 = 0$. As result, we find

$$\tau = \frac{M_1^N - \beta_1\beta_2 M_2^N + r\beta_1(M_2^N - M_1^N)}{1 - \beta_1\beta_2}, \tag{34}$$

$$r = \beta_2 \frac{M_2^N - M_1^N}{M_1^N - \beta_2\beta_1 M_2^N}. \tag{35}$$

The frequency dependence of the reflection coefficient $R = |r|^2$ is shown in Fig. 5 for different magnetic fields H_{ab} [in (a)], y-axis wave vectors q [in (b)], and sample lengths l [in (c)]. The reflection R strongly depends on the frequency ω. The average transparency (transmission T) of the crystal increases when increasing the frequency $\tilde{\omega}$. The dependence $R(\omega)$ has characteristic interference minima arising due to the interference of the transmitted and reflected waves.[26] The reflection R (or transmission T) of the EMWs strongly depends on the in-plane magnetic field, as shown in Fig. 5. Thus, we predict a giant magneto-optical effect. The average transmission T reduces fast when increasing H_{ab} due to an increase in the number of scatterers in the sample. For the same reason, the positions, number, and the sharpness of the interference peaks in $R(\omega)$ also changes with H_{ab}. Finally, R becomes flatter and approaches one for large enough H_{ab}. It follows from the results presented in Fig. 5(b), that waves with higher q pass through the system easier than waves with lower q. This feature is also intuitively clear since, with growing q, the wavelength in the y direction becomes closer to the characteristic interlayer distance. Waves with higher q are more sensitive to the magnetic field variations, as shown in Fig. 5(a) and 5(b), since the value of κ_0 in Eq. (27) increases when growing q and the interaction of EMWs with JVs becomes stronger. Close to the forbidden frequency zones, the dependence of R and T versus ω at $q \neq 0$ has several characteristic deep and narrow peaks. At $q = 0$ the corresponding functions are monotonous.

The average transparency of the sample also increases when diminishing the sample thickness, as shown in Fig. 5(c), since the growth of l gives rise to an increase in the number and sharpness of the interference peaks in $R(\omega)$. We should emphasize that varying the applied magnetic field H_{ab} tunes the reflection, all the way from 0 to 1, at a given frequency. In a long sample this tuning remains significant even at small q, due to the cumulative effect of a large number of weak scatterers.

B. Electromagnetic waves incident from the vacuum

Here, we consider a wave incident from the vacuum to a sample edge, as shown in Fig. 4(b). The wave incident to the sample surface parallel to the ab planes can be studied by using the same method.

In the case under study, the wave vector q is the same in the vacuum and in the sample since the normal component of the electric induction, εE_x, is continuous at the sample edge. As a result, the value of the parameter qs should be small for THz-range radiation. Naturally, the dispersion relation for the wave (1) in vacuum reads $k^2 + q^2 = \omega^2/c^2$. For $\omega/2\pi = 1$ THz the corresponding wavelength is 0.3 mm, while s is in the nanometer range. For $s = 2$ nm we find the estimate $qs \leqslant 4.19 \times 10^{-5}$. Thus, we assume below that $q = 0$, resulting in the magnetic field and the y component of the electric field of JPWs to be related to the gauge-invariant phase by simple equations[18,19]

$$H = \frac{\Phi_0}{2\pi s}\frac{\partial \varphi}{\partial x}, \quad E_y = \frac{\Phi_0}{2\pi sc}\frac{\partial \varphi}{\partial t}. \tag{36}$$

We present the EMW in vacuum in the form $H = H_0(e^{ik_0x - i\omega t} + re^{ik_0x + i\omega t})$ at the left of the sample and

$H=H_0\tau e^{ik_0x-i\omega t}$ at the right of it. Imposing the continuity of both H and E_y at the sample surface we find

$$1+r=-\frac{i\varepsilon\kappa_1}{4\pi h_{ac}}(C_{10}^1e^{-i\kappa_1 b}-C_{10}^2e^{i\kappa_1 b}),$$

$$1-r=-\frac{i\varepsilon\omega\gamma s}{4\pi ch_{ac}}(C_{10}^1e^{-i\kappa_1 b}+C_{10}^2e^{i\kappa_1 b}),$$

$$\tau=-\frac{i\varepsilon\kappa_1}{4\pi h_{ac}}(C_{1N}^1-C_{1N}^2),$$

$$\tau=-\frac{i\varepsilon\omega\gamma s}{4\pi ch_{ac}}(C_{1N}^1+C_{1N}^2). \tag{37}$$

Now, using Eq. (33), we find the expression for the amplitude r of the reflected wave

$$r=\frac{1+Z(\tilde{\omega})D(\tilde{\omega})\exp(-2i\kappa_1 b)}{Z(\tilde{\omega})+D(\tilde{\omega})\exp(-2i\kappa_1 b)},$$

$$D=\frac{\beta_1(Z+\beta_2)M_2^N-(1+\beta_1 Z)M_1^N}{(Z+\beta_2)M_2^N-\beta_2(1+\beta_1 Z)M_1^N}, \tag{38}$$

where

$$g=\frac{s}{\sqrt{\varepsilon}\lambda_{ab}},\quad Z=\frac{\kappa_1-i\tilde{\omega}g}{\kappa_1+i\tilde{\omega}g}. \tag{39}$$

The reflection coefficient is $R=|r|^2$, while the transmission coefficient is $T=|\tau|^2=1-R$. The distance between the sample edge and the nearest JV row is b. Note that the "effective impedance" Z describes EMW scattering at the sample boundaries. Also, Eq. (34) for internally propagating waves with $q=0$, can be reproduced by setting $Z=0$ in Eq. (38). In the absence of an applied magnetic field, i.e., no vortices $N=0$ in the sample, it can be readily seen from Eqs. (38) and (39) that the reflection coefficient becomes zero under usual interference conditions $\kappa_1 l=\pi m$, where m is an integer.

The calculated frequency dependence of the reflection coefficient is shown in Fig. 6 for $q=0$ at different magnetic fields and different sample lengths. The average transparency increases when increasing the frequency and with the decrease of the number of scattering layers, due to a decrease of either the magnetic field H_{ab} or the sample length. As in the case $H_{ab}=0$, the oscillations in the transition and reflection coefficients occur due to the interference of the scattered and transmitted waves on JVs and sample boundaries. These transmission and reflection coefficients can be easily tuned by the in-plane magnetic field H_{ab}. For standard parameters for Bi2212 single crystals, varying the applied magnetic field within a range of 100 Oe *can drastically change the transparency* of a sample of length of about 1 mm in the x direction.

Next, we examine how dissipation, which was omitted in Ref. 14, affects reflectivity. The effect of dissipation is illustrated in Fig. 6(c). When increasing $\tilde{\omega}_r$, the curves $R(\omega)$ become smoother: the minima of the reflection coefficient moves up while the maxima goes down. However, a considerable effect of the dissipation is obtained only at high values of $\tilde{\omega}_r$ in the range of 0.01 and higher.

V. EFFECT OF THE JOSEPHSON VORTEX LATTICE MOTION

In contrast to the usual fixed periodic arrays of scatterers in optics, the JV vortex structure can be easily driven, e.g., by applying a transport current in the direction perpendicular to the superconducting layers. The amplitude and the frequency of the current could serve as an additional control "knob" allowing a more versatile tuning of the EMW propagation in layered superconducting structures. Moreover, the effect of the motion of periodic structures on the spectrum of the photonic crystal has not been discussed so far for any kind of photonic crystals.

We assume below that a constant uniform current $J_\perp$ flows in the y direction and, as a result, the JVs move with a constant velocity v in the x direction. We also assume that the vortex velocity is smaller than the critical value $v_c=\gamma s\omega_J$, since the moving JV becomes unstable[8] when v exceeds v_c. In this limit, we neglect effects of order v/c, where c is the speed of light. For simplicity, in this section we only consider the case $\omega>\omega_J$ and $\omega_r=0$.

For a moving JV lattice, we now seek a solution for the gauge-invariant phase difference of EMW's in the form

$$\varphi_1(x,y,t)=\psi(x-vt)\exp(iqy-i\omega' t). \tag{40}$$

The value ω' now corresponds to the frequency of the waves in the coordinate system moving with velocity v with the respect to the superconducting medium. Equation (18), for ψ in the long-wavelength limit, now reads

$$\psi''(\zeta)-2i\kappa_v^2(q)\tilde{\omega}'V\psi'(\zeta)-\kappa_v^2(q)[\tilde{\omega}_J^2(\zeta)-\tilde{\omega}'^2]\psi(\zeta)=0, \tag{41}$$

where $\tilde{\omega}'=\omega'/\omega_J$, $''$ denotes the second derivative differentiation with respect to $\zeta\equiv\eta-Vt\omega_J$,

$$\kappa_v^2(q)=\frac{\kappa_0^2(q)}{1-\kappa_0^2(q)V},\quad V=\frac{v}{v_c}=\frac{v\omega_J}{\gamma s}. \tag{42}$$

In analogy to Eq. (29), the solution of Eq. (41) for each jth cell of the periodic JV structure can be expressed as

$$\vec{\psi}_j=\{C_{1j}^l\exp(ip_{1l}\zeta);\ C_{2j}^l\exp(-ip_{2l}\zeta)\}, \tag{43}$$

where

$$p_{1l,2l}=k_v\pm\kappa_{lv},\quad \kappa_{lv}^2=\kappa_l^2+k_v^2,\quad k_v=\tilde{\omega}'\kappa_v^2V. \tag{44}$$

It is seen from Eqs. (41)–(44) that the most pronounced effect of the JV lattice motion, with $v\ll v_c$, should be expected at large transverse wave vectors q, when $q^2\lambda_{ab}^2\gg 1$, and the value $\kappa_0^2(q)V$ is not too small compared to unity.

A. Band-gap structure for a moving Josephson vortex lattice: Doppler effect in tunable photonic crystals

Following the approach described in Sec. III, we use Bloch's theorem to find the band-gap structure and present

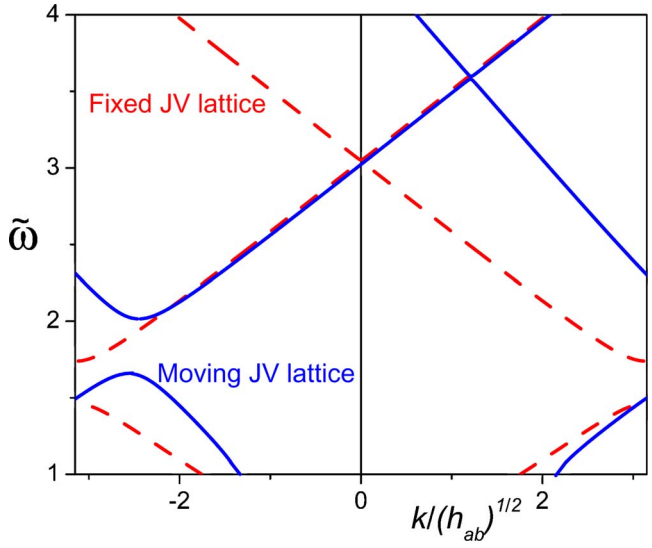

FIG. 7. (Color online) Band-gap structure for the moving JV lattice. The dependence of $\tilde{\omega}$ versus $k/\sqrt{h_{ab}}$ at $h_{ab}=0.2$ and $qs=0.3\pi$: $V=0$ (red dashed line), $V=0.2$ (blue solid line). Other parameters are the same as in Fig. 3.

$\psi(\zeta)$ in the form of a Bloch wave $\psi(\zeta)=u(\zeta,k)\exp(ik\zeta)$, where $u(\zeta)$ is a periodic function with the period $1/\sqrt{h_a}b=1+b$ and k is in the first Brillouin zone, $-\pi\sqrt{h_{ab}}<k<\pi\sqrt{h_{ab}}$. Using the continuity of ψ and ψ' and the periodicity of $u(\zeta)$, we find the equation for $\tilde{\omega}'(k)$ analogous to Eq. (27)

$$\cos(\kappa_{1v}b)\cos(\kappa_{2v}) - \frac{\kappa_{1v}^2+\kappa_{2v}^2}{2\kappa_{1v}\kappa_{2v}}\sin(\kappa_{1v}b)\sin(\kappa_{2v}) = \cos[(k-k_v)(b+1)], \tag{45}$$

where $\kappa_{lv}(\tilde{\omega}')$ and $k_v(\tilde{\omega}')$ are functions of the frequency $\tilde{\omega}'$ in the moving coordinate system. In analogy to the Doppler effect, in order to find the function $k(\tilde{\omega})$ in the fixed coordinate system, we should use a transformation of the frequency

$$\tilde{\omega}=\tilde{\omega}'+[k_v(\tilde{\omega}')+\kappa_{1v}(\tilde{\omega}')]V. \tag{46}$$

Note that the frequencies in the superconducting medium located between vortices ($l=1$) and inside the JVs cores ($l=2$) are different in the fixed coordinate system. We choose κ_{1v} in Eq. (46) since we are interested in the dependence of $\tilde{\omega}(k)$ for the medium itself (between vortices).

The results of the solution of Eqs. (45) and (46) are shown in Fig. 7 for different values of $V\ll 1$. The curves $\tilde{\omega}(k)$ become deformed and are asymmetrical with respect to the sign of the velocity v. Indeed for $v\neq 0$, the spectrum is shifted either to the left or to the right, depending on the sign of v due to the Doppler effect. The influence of the lattice motion is most pronounced in the vicinity of the frequency gap. The effect of the motion of the JVs on the spectrum disappears at small q, when $\kappa_0^2(q)V\ll 1$.

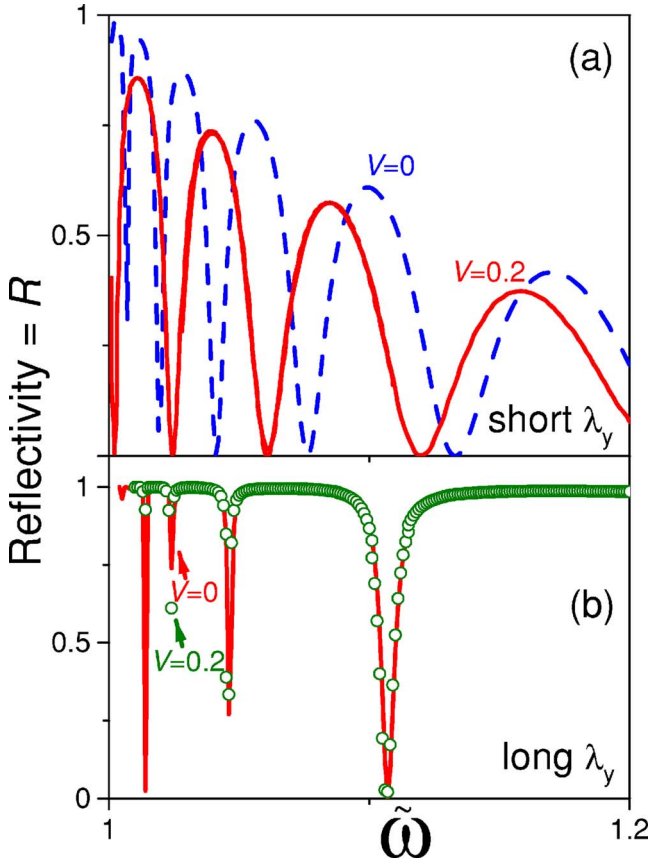

FIG. 8. (Color online) Reflection coefficient $R(\omega)$ for EMWs propagating inside the sample with JV lattices moving with (normalized) velocity V. The sample length is $l=100\gamma s$ and $h_{ab}=6.25\times 10^{-2}$. (a) $qs=0.3\pi$, $V=0$ (blue dashed line), and $|V|=0.2$ (solid red line); (b) $qs=0.05\pi$, $V=0$ (solid red line), $|V|=0.2$ (green open circles). Other parameters are the same as in Fig. 5.

B. Reflection of electromagnetic waves by a moving Josephson vortex lattice

First we discuss the reflection of EMWs propagating inside the sample. In this case EMWs do not scatter by fixed sample boundaries, and the solution (43) allows us to directly find the reflection and transmission coefficients. Using the approach described in Sec. IV, we find that the frequency dependence of the reflection coefficient $R=|r|^2$ is described by Eqs. (34) and (32), where we should replace $\kappa_l(\tilde{\omega})$ by $\kappa_{lv}(\tilde{\omega}')$. The frequency of the incident wave is defined by Eq. (46), while the frequency of the reflected wave is shifted by $\Delta\tilde{\omega}=2\kappa_{1v}(\tilde{\omega}')V$, which is the *analog of the Doppler effect*. For example, if $qs=0.3/\pi$ and $v=0.1v_c$, the value of the frequency shift is about 20% of ω_J.

The reflection coefficient R as a function of the incident wave frequency $\tilde{\omega}$ is shown in Fig. 8 for different values of V and q. It is clearly seen from this figure that the effect of the JV lattice motion is of importance only for EMWs having high enough q. The JV lattice motion changes the positions of the transparency windows and increases the average transparency. The strength of this effect is independent of the direction of motion, i.e., of the direction of the driving current.

In the case of EMWs propagating from the vacuum, EMWs scattering at the fixed sample boundaries results in the excitation of waves with frequencies different than the one described in Eq. (43), i.e., waves with different time dependence. This problem can be solved by the method described in Sec. IV only in the limiting case of a large number of JVs in the sample, i.e., $N \gg 1$. However, as mentioned in Sec. IV, EMWs having $q\lambda_{ab} \gg 1$ and THz-range frequency cannot propagate in the vacuum. Thus, the effect of the JV lattice motion is negligible in this case. For example, the frequency shift $\Delta\omega$ for such waves is of the order of $\omega_J(s/\lambda_{ab})^2(v/v_c)$.

VI. CONCLUSIONS

Electromagnetic waves in layered superconductors can propagate if their frequency exceeds the Josephson plasma frequency that usually lies in the THz or sub-THz frequency range. Josephson vortex lattices are easily tunable periodic arrays that scatter EMWs. Here we demonstrate that the scattering of EMWs by a JV array produces a *tunable band gap structure* or THz photonic crystal. The variation of the in-plane magnetic field easily tunes the parameters of the photonic crystal, in particular the value and the position of the forbidden gaps. Another possibility, also unusual for standard photonic crystals, is to influence the photonic crystal parameters by moving the JV periodic array driven by the transport current in the direction across the superconducting layers.

The scattering of EMWs by a periodic array results in the strong dependence of its reflection and transmission coefficients on both the applied in-plane magnetic fields and transport currents. A relatively small change (about 10–100 Oe) in the applied in-plane magnetic field can switch the sample from fully transparent to fully reflected regimes within given frequency windows. As a result, the optical characteristics of the layered sample can be conveniently tuned by the in-plane magnetic field. This phenomenon could be referred to as a giant magneto-optical effect, in analogy to the traditional magneto-optical effect[16] found in magnetic media. If the transverse wave vector of EMWs is large enough, $q^2\lambda_{ab}^2 \gg 1$, an analogous effect could be achieved by applying a transverse current, in analogy to the Doppler effect in standard wave physics.

The effects described here could be used in developing THz filters and "glass/mirrors" switches. The advantage of these devices is their tunability by magnetic or electric fields.

ACKNOWLEDGMENTS

We acknowledge partial support from the NSA, LPS, ARO, by the Grants NSF No. EIA-0130383, No. JSPS-RFBR 06-02-91200, and No. RFBR 06-02-16691. S.S. acknowledges support from the Ministry of Science, Culture and Sport of Japan via the Grant-in-Aid for Young Scientists No. 18740224, the EPSRC via No. EP/D072581/1, and the AQDJJ network.

[1] J. Zitzmann, A. V. Ustinov, M. Levitchev, and S. Sakai, Phys. Rev. B **66**, 064527 (2002).
[2] Y. Tominari, T. Kiwa, H. Murakami, M. Tonouchi, H. Wald, P. Seidel, and H. Schneidewind, Appl. Phys. Lett. **80**, 3147 (2002).
[3] M. Tachiki, M. Iizuka, K. Minami, S. Tejima, and H. Nakamura, Phys. Rev. B **71**, 134515 (2005); Physica C **437-438**, 299 (2006).
[4] G. Hechtfischer, R. Kleiner, A. V. Ustinov, and P. Müller, Phys. Rev. Lett. **79**, 1365 (1997).
[5] See, e.g., the special issue of Philos. Trans. R. Soc. London **362**(1815), 1 (2004).
[6] V. M. Krasnov, Phys. Rev. B **63**, 064519 (2001); R. G. Mints and I. B. Snapiro, *ibid.* **52**, 9691 (1995).
[7] E. Goldobin, A. Wallraff, N. Thyssen, and A. V. Ustinov, Phys. Rev. B **57**, 130 (1998).
[8] S. Savel'ev, V. Yampolskii, A. Rakhmanov, and F. Nori, Phys. Rev. B **72**, 144515 (2005); Physica C **437-438**, 281 (2006).
[9] A. A. Abdumalikov, Jr., M. V. Fistul, and A. V. Ustinov, Phys. Rev. B **72**, 144526 (2005).
[10] I. Kakeya, T. Wada, K. Kadowaki, and M. Machida, Physica C **378-381**, 347 (2002).
[11] T. Koyama, Phys. Rev. B **68**, 224505 (2003); H. Matsumoto and T. Koyama, Physica C **412-414**, 444 (2004).
[12] Y. Matsuda, M. B. Gaifullin, K. Kumagai, K. Kadowaki, T. Mochiku, and K. Hirata, Phys. Rev. B **55**, R8685 (1997).
[13] S. Savel'ev, V. Yampolskii, A. L. Rakhmanov, and F. Nori, Physica C **445-448**, 175 (2006).
[14] S. Savel'ev, A. L. Rakhmanov, and F. Nori, Phys. Rev. Lett. **94**, 157004 (2005); Physica C **445-448**, 180 (2006).
[15] H. Susanto, E. Goldobin, D. Koelle, R. Kleiner, and S. A. van Gils, Phys. Rev. B **71**, 174510 (2005).
[16] H. Ebert, Rep. Prog. Phys. **59**, 1665 (1996).
[17] A. E. Koshelev, Phys. Rev. Lett. **83**, 187 (1999); Phys. Rev. B **68**, 094520 (2003); Physica C **408-410**, 470 (2004); J. Mirković, S. E. Savel'ev, E. Sugahara, and K. Kadowaki, Phys. Rev. Lett. **86**, 886 (2001); S. E. Savel'ev, J. Mirković, and K. Kadowaki, Phys. Rev. B **64**, 094521 (2001); Physica C **357-360**, 597 (2001); **378-381**, 580 (2002); S. Savel'ev, J. Mirković, and F. Nori, *ibid.* **388**, 653 (2003); S. Savel'ev and F. Nori, Nat. Mater. **1**, 179 (2002); D. Cole, S. Bending, S. Savel'ev, A. Grigorenko, T. Tamegai, and F. Nori, *ibid.* **5**, 305 (2006); A. Tonomura, *ibid.* **5**, 257 (2006); S. Savel'ev and F. Nori, Physica C **437-438**, 226 (2006); D. Cole, J. S. Neal, M. R. Connolly, S. J. Bending, S. Savel'ev, F. Nori, M. Tokunaga, and T. Tamegai, *ibid.* **437-438**, 52 (2006); J. Mirković, S. Savel'ev, H. Sato, F. Nori, and K. Kadowaki, New J. Phys. **8**, 226 (2006).
[18] A. Barone and G. Paterno, *Physics and Applications of the Josephson Effect* (Wiley, New York, 1982).
[19] S. N. Artemenko and S. V. Remizov, Physica C **362**, 200 (2001).
[20] A. E. Koshelev, Phys. Rev. B **62**, R3616 (2000).
[21] Yu. I. Latyshev, A. E. Koshelev, and L. N. Bulaevskii, Phys. Rev. B **68**, 134504 (2003).
[22] S. Savel'ev, V. A. Yampolskii, A. L. Rakhmanov, and F. Nori, Nat. Phys. **2**, 521 (2006).

[23] T. Koyama and M. Tachiki, Phys. Rev. B **54**, 16183 (1996).
[24] S. Savel'ev, V. Yampol'skii, and F. Nori, Phys. Rev. Lett. **95**, 187002 (2005); Physica C **445-448**, 183 (2006).
[25] A. Gurevich, Phys. Rev. B **46**, R3187 (1992).
[26] L. D. Landau, E. M. Lifshitz, and L. P. Pitaevskii, *Electrodynamics of Continuous Media* (Butterworth-Heinemann, Oxford, 1995).
[27] In Ref. 8 we use the approximation (23) with the numerical coefficient $3/2$ instead of π.
[28] E. Yablonovitch, Phys. Rev. Lett. **58**, 2059 (1987).
[29] S. G. Johnson and J. D. Joannopoulos, *Photonic Crystals: The Road from Theory to Practice* (Springer, New York, 2002).
[30] J. D. Joannopoulos, R. D. Meade, and J. N. Winn, *Photonic Crystals* (Princeton University Press, Princeton, 1995).
[31] R. E. Slusher and B. J. Eggleton, *Nonlinear Photonic Crystals* (Springer, New York, 2003).
[32] K. Sakoda, *Optical Properties of Photonic Crystals* (Springer, New York, 2001).